Reduced Edge Instability and Improved Confinement in the MST Reversed-Field Pinch

B. E. Chapman,[1,*] J. K. Anderson,[1] T. M. Biewer,[1] D. L. Brower,[2] S. Castillo,[1] P. K. Chattopadhyay,[1] C.-S. Chiang,[1] D. Craig,[1] D. J. Den Hartog,[1] G. Fiksel,[1] P. W. Fontana,[1] C. B. Forest,[1] S. Gerhardt,[1] A. K. Hansen,[1] D. Holly,[1] Y. Jiang,[2] N. E. Lanier,[1] S. C. Prager,[1] J. C. Reardon,[1] and J. S. Sarff[1]

[1]*University of Wisconsin, Madison, Wisconsin 53706*
[2]*University of California, Los Angeles, California 90095*

(Received 18 January 2001; published 24 October 2001)

Improved confinement has been achieved in the MST through control of the poloidal electric field, but it is now known that the improvement has been limited by bursts of an edge-resonant instability. Through refined poloidal electric field control, plus control of the toroidal electric field, we have suppressed these bursts. This has led to a total beta of 15% and a reversed-field-pinch-record estimated energy confinement time of 10 ms, a tenfold increase over the standard value which for the first time substantially exceeds the confinement scaling that has characterized most reversed-field-pinch plasmas.

DOI: 10.1103/PhysRevLett.87.205001 PACS numbers: 52.55.Hc, 52.25.Fi, 52.25.Gj

The reversed-field-pinch (RFP) plasma is susceptible to large-amplitude magnetic fluctuations [1]. The dominant fluctuations have poloidal mode number $m = 1$ and are resonant in the plasma core at locations where the wave number parallel to the magnetic field vanishes. These fluctuations grow to an amplitude sufficient to cause reconnection and stochastization of the magnetic field lines, thereby degrading energy confinement. The primary driver of these fluctuations is the naturally occurring radial gradient in the current flowing parallel to the magnetic field [1]. With the goal of modifying this gradient in Madison Symmetric Torus (MST) [2] RFP plasmas, inductive auxiliary parallel current drive was applied in the plasma edge [3–6]. Comprised of a poloidal electric field induced by a transient change in the toroidal flux in the plasma, this technique resulted in a reduction of the $m = 1$ fluctuations and an increase in the global energy confinement time from the MST standard 1 ms to 5 ms.

In this Letter, we report two advances in the understanding and control of magnetic fluctuations and energy transport. First, we report that the previously achieved $m = 1$ fluctuation reduction and confinement improvement were limited by bursts of edge-resonant $m = 0$ magnetic fluctuations that were observed in conjunction with the auxiliary current drive [3–7]. The $m = 1$ fluctuations account for the bulk of energy transport in standard MST plasmas [8]. Thus, the $m = 0$ fluctuations have not previously been considered to play a significant role in transport. Second, we report that we can now suppress these bursts, resulting in an additional improvement in energy confinement. Burst suppression is achieved through improved control of the surface parallel electric field, through manipulation of both the poloidal and toroidal electric fields [7]. This has allowed a further reduction of the $m = 1$ fluctuations, along with suppression of the $m = 0$ bursts, for up to the duration of the current drive. With simultaneous control of core and edge fluctuations, the central electron temperature increases substantially, reaching a maximum of 1.28 keV at high toroidal plasma current (480 kA). At low current (210 kA) the total beta reaches about 15% with an estimated energy confinement time of 10 ms, which is a tenfold increase over the MST standard confinement time and which substantially exceeds for the first time the confinement scaling that has characterized most RFP plasmas.

The ohmically heated MST plasma has major and minor radii of 150 cm and 51 cm, respectively, and is fueled with deuterium. The electric and magnetic field waveforms from a typical discharge with auxiliary parallel current drive are shown in Fig. 1. The surface (i.e., at the plasma boundary) poloidal and toroidal electric fields, $E_\theta(a)$ and $E_\phi(a)$, are shown in Figs. 1(a) and 1(b). The surface poloidal and toroidal magnetic fields, $B_\theta(a)$ and $B_\phi(a)$, are shown in Fig. 1(c). Shown in Fig. 1(d) is the surface parallel electric field, $E_\parallel(a) = \mathbf{E} \cdot \mathbf{B}/B = (E_\theta B_\theta + E_\phi B_\phi)/B$, where B is the total magnetic field, and all terms are surface quantities. The poloidal current drive consists of five consecutive pulses, beginning at 9 ms in Fig. 1. The toroidal electric field is reversed at 16 ms. The first two E_θ pulses in Fig. 1(a) are obscured by negative-going bursts associated with the bursts of $m = 0$ fluctuations. The $m = 0$ bursts induce a response in $E_\theta(a)$ since they correspond to the generation of toroidal magnetic flux within the plasma.

That the bursts in $E_\theta(a)$ are associated primarily with $m = 0$ magnetic fluctuations (modes), and not the core-resonant $m = 1$ modes, is illustrated in Fig. 2, which shows an expanded view of the bursts occurring in Fig. 1 from about 9.5 to 11.5 ms. Each burst in $E_\theta(a)$, Fig. 2(a), has a counterpart in the $m = 0$ modes, Fig. 2(b), all of which are resonant at the toroidal magnetic field reversal radius in the plasma edge. The bursts often have no discernible counterpart in the $m = 1$ modes, Fig. 2(c). In the cases in which there is a burst-like increase of the $m = 1$ modes, such as at 11 and 11.3 ms, it follows the increase in the $m = 0$ modes and is broader in time. Following the last $m = 0$ burst, both $m = 0$ and $m = 1$

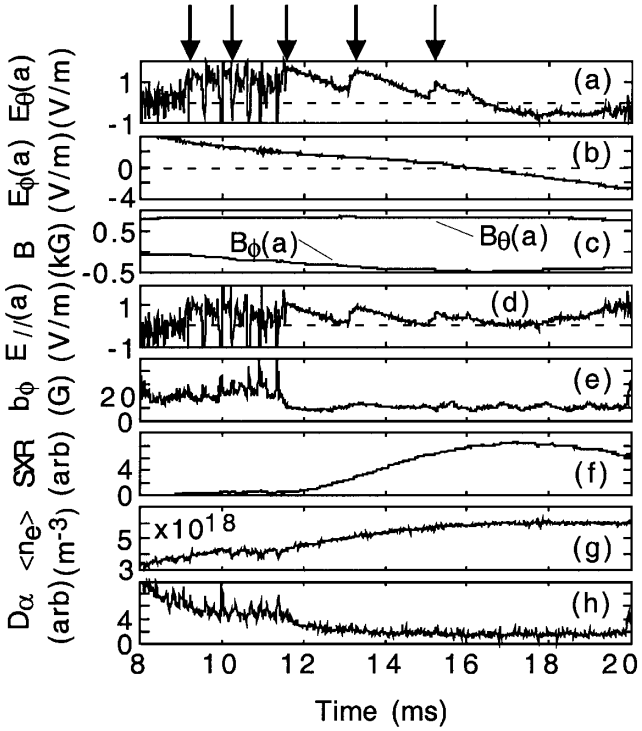

FIG. 1. Surface (a) poloidal and (b) toroidal electric fields, (c) surface poloidal and toroidal magnetic fields, (d) surface parallel electric field, (e) rms fluctuation in the toroidal magnetic field, including $m = 0$ and $m = 1$ modes, toroidal mode numbers 1–15, (f) soft x-ray emission, (g) central line-averaged electron density, and (h) radiation from neutral deuterium atoms. Peaks of poloidal electric field pulses indicated by arrows. Toroidal plasma current is 210 kA.

mode amplitudes exhibit a multi-ms reduction. Such a sustained $m = 1$ reduction occurs only after the $m = 0$ bursts are suppressed. Thus, control of edge-resonant instability is essential to the improved confinement plasmas described here.

We have established that multi-ms $m = 0$ burst suppression is aided by maintaining $E_{\|}(a) \geq 0$. This has been achieved by adjusting the spacing of the E_θ pulses to prevent decay of $E_\theta(a)$ to zero between pulses and by reversing $E_\phi(a)$ following the last E_θ pulse. This improved control of E_θ necessitates a significant change in $|B_\phi(a)|$, Fig. 1(c), which increases by an order of magnitude and peaks at about 60% of $B_\theta(a)$. This increase allows E_ϕ reversal to contribute significantly to $E_{\|}(a)$. During poloidal current drive at 210 kA, the reversal parameter, $F \equiv B_\phi(a)/\langle B_\phi \rangle$, drops from -0.13 to -2.1, where $\langle B_\phi \rangle$ is a cross-section average. The pinch parameter, $\Theta \equiv B_\theta(a)/\langle B_\phi \rangle$, increases from 1.7 to 3.5.

A multi-ms period of core and edge fluctuation reduction, brought about by suppression of the $m = 0$ bursts, begins at about 11.5 ms in Fig. 1. The data in Figs. 1(e)–1(h) illustrate the changes in the plasma that contribute to improved energy and particle confinement. In Fig. 1(e) is the rms sum of the $m = 0$ and $m = 1$ fluctuations discussed in Fig. 2. Periods of reduced fluc-

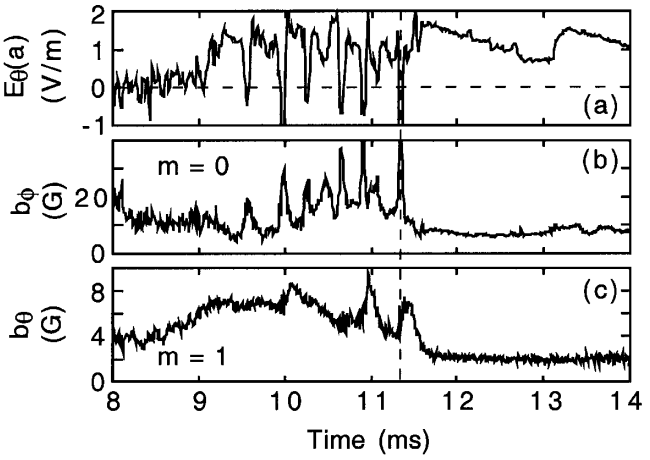

FIG. 2. From the discharge in Fig. 1, (a) surface poloidal electric field, (b) rms fluctuation in the toroidal magnetic field, including only $m = 0$ modes, toroidal mode numbers 1–5, and (c) rms fluctuation in the poloidal magnetic field, including only $m = 1$ modes, toroidal mode numbers 6–15.

tuations like that shown here have been sustained for up to 10 ms. Accompanying this fluctuation reduction is a rapid rise in the electron temperature, T_e, illustrated qualitatively in Fig. 1(f), which contains soft x-ray emission from the plasma. The evolution shown here is in rough agreement with limited measurements of the time-evolving central electron temperature, described below. The temperature increase is accompanied by a decrease in the Ohmic input (electron heating) power, also discussed below. The central line-averaged density, $\langle n_e \rangle$ [Fig. 1(g)], also increases with burst suppression, and there is a concurrent decrease in the radiation from recycled neutral deuterium atoms, Fig. 1(h), which indicates a decrease in the particle source rate.

With burst suppression, T_e increases substantially over much of the plasma. Profiles of T_e in standard- and improved-confinement plasmas with toroidal plasma currents $I_\phi \sim 200$ and ~ 400 kA are shown in Fig. 3. The data at $\rho < 0.9$ (where ρ is the normalized minor radius in flux coordinates) were measured with a Thomson scattering diagnostic, while the data at $\rho > 0.9$, Fig. 3(a), were measured with a Langmuir probe. All of the data points are averages of measurements from many similar plasmas. The standard profiles were measured between sawtooth crashes (which correspond to a large, global increase in fluctuations) at the peak of the plasma current when the plasma is hottest and densest. The improved-confinement profiles were compiled at 18 ms in plasmas like that in Fig. 1. This is the time at which the central electron temperature peaks. In addition to the significant increase in the core temperature, there is a simultaneous decrease in the edge temperature, Fig. 3(a), and density (not shown).

The estimated energy confinement time, $\tau_E \equiv W_{\rm th}/(P_{\rm oh} - dW_{\rm th}/dt)$, increases by up to a factor of 10 with burst suppression. Here, $W_{\rm th} \equiv (3/2) \int (n_e T_e + n_i T_i)\, dV$ is the volume-integrated plasma thermal energy,

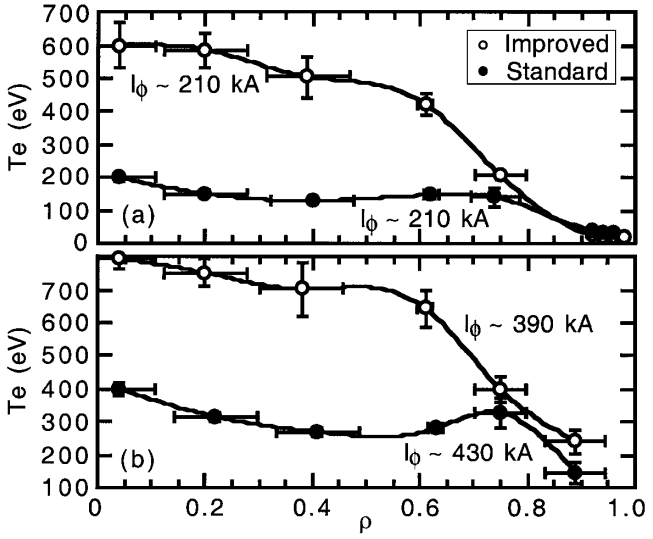

FIG. 3. Electron temperature profiles from standard- and improved-confinement plasmas with a central line-averaged density of (a) $\sim 8 \times 10^{18}$ m^{-3} and (b) 1×10^{19} m^{-3}. Horizontal bars on Thomson scattering data points ($\rho < 0.9$) indicate the radial extent over which the diagnostic integrates.

n_i and T_i are the ion density and temperature, and $P_{\rm oh}$ is the Ohmic input power. The energy confinement time and its constituents are compared in Table I for standard- and improved-confinement plasmas. At 390 kA, τ_E is estimated to reach 8.8 ms. At 210 kA it reaches 10.1 ms, the largest value yet achieved in the RFP and a tenfold increase over the MST standard 1 ms, which is a time average including the time between and during sawtooth crashes. The estimated global electron particle confinement time, τ_P, measured at 210 kA, increases eightfold (Table I) [9].

Although the density increases with improved confinement [Fig. 1(g)], standard- and improved-confinement plasmas are compared at similar densities by applying auxiliary current drive to plasmas with an initially reduced density. The electron density profile, measured with a multichord interferometer, is fairly flat in both types of plasma [9], and the ion density profile is assumed identical to the electron density profile. The central electron temperatures, $T_e(0)$, listed in Table I are extracted from the profiles in Fig. 3. We also measured the central temperature in 480 kA improved-confinement plasmas with $\langle n_e \rangle \sim 9 \times 10^{18}$ m^{-3}. The resulting 1.28 keV, achieved with exceptionally long burst-free periods, is a new high for the RFP. The central ion temperature, $T_i(0)$, was measured with Rutherford scattering, a neutral-beam-based technique [10]. In the 210 and 430 kA standard plasmas, $T_i(0) = (0.75)T_e(0)$. In 210 kA improved-confinement plasmas, $T_i(0) = (0.3)T_e(0)$, while at 390 kA, $T_i(0) = (0.5)T_e(0)$. The collisional energy transfer time between electrons and ions is tens of ms in these plasmas, so the rapid increase in T_e with improved confinement is not reflected in T_i. Lacking T_i profile measurements, we assume the above ratios for the ion temperature profile, e.g., $T_i(r) = (0.75)T_e(r)$ in standard plasmas.

TABLE I. Parameters, defined in the text, from discharges with standard and improved confinement. Standard data measured between sawtooth crashes, except for τ_E, where values between crashes and including crashes are shown. Improved-confinement $\langle n_e \rangle$, $T_e(0)$, $\beta_{\rm tot}$, and β_θ quoted at 18 ms, when they peak, while $dW_{\rm th}/dt$ quoted from 16–18 ms and $P_{\rm oh}$, τ_P, and τ_E quoted at 17 ms, with an estimated uncertainty of ± 2.5 ms for τ_E.

	Standard	Imp.	Standard	Imp.
I_ϕ (kA)	210	210	430	390
$\langle n_e \rangle$ (10^{19} m^{-3})	0.8	0.7	1.0	1.0
$T_e(0)$ (eV)	200	600	400	792
$dW_{\rm th}/dt$ (MW)	0	0.47	0	0.55
$P_{\rm oh}$ (MW)	2.0	1.0	4.0	2.0
τ_E (ms)	1.4/1.0	10.1	1.6/1.0	8.8
τ_P (ms)	0.6	4.7	?	?
$\beta_{\rm tot}$ (%)	9.0	15.4	4.8	10.7
β_θ (%)	9.0	18.1	4.8	11.8

The Ohmic input power drops by a factor of 2 with improved confinement (Table I). In standard plasmas, the Ohmic input power, $P_{\rm oh}$, is calculated through global power balance, where $P_{\rm oh} \equiv P_{\rm in} - dW_m/dt$, $P_{\rm in}$ is the total input power, and W_m is the magnetic energy stored in the plasma. The total input power is the accurately measured Poynting flux at the plasma surface, and the relatively small dW_m/dt is obtained from equilibrium modeling using measurements of the surface magnetic field. In the improved-confinement plasmas described here, $dW_m/dt \sim P_{\rm in}$, and we lack the magnetic field profile data required to accurately resolve the difference between these two terms. Thus, we estimate $P_{\rm oh}$ for improved confinement through the volume integral $\int \eta J^2\, dV$, where J is the current density, $\eta \propto Z/T_e^{3/2}/(1 - f_t)$ is the plasma resistivity, Z is calculated from $Z_{\rm eff}$, the mean ionic charge, and f_t is the trapped particle fraction. J and f_t are estimated at a single point in time with MSTFit [11], a toroidal equilibrium code whose calculations are constrained by measurements of, e.g., the pressure profile, the edge current profile, and the on-axis magnetic field (the latter measured with a motional-Stark-effect diagnostic [12]).

As an estimate of $Z_{\rm eff}$ in improved-confinement plasmas, we adopt a value estimated in standard plasmas from a comparison of $P_{\rm oh}$ calculated through power balance and $\int \eta J^2\, dV$ calculated with MSTFit. For example, we know from power balance that $P_{\rm oh} = 4.0$ MW at 430 kA in standard plasmas (Table I). MSTFit requires $Z_{\rm eff} = 2.0$, assumed spatially constant, to arrive at $\int \eta J^2\, dV = 4.0$ MW. The same comparison for the 210 kA standard plasmas yields $Z_{\rm eff}$ slightly lower than 2.0. This value is consistent with an upper-bound estimate of the central $Z_{\rm eff}$ provided by the Rutherford-scattering diagnostic [10]. For the improved-confinement plasmas, we thus assume $Z_{\rm eff} = 2.0$ for both 210 and 390 kA.

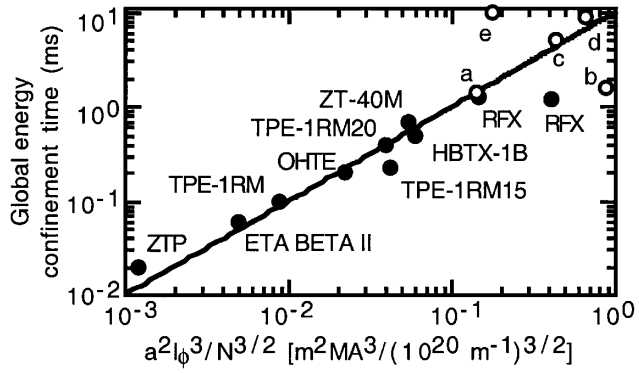

FIG. 4. Confinement results from various RFP devices and (*a*) MST 210 kA standard, (*b*) MST 430 kA standard, (*c*) previous MST 340 kA improved confinement, (*d*) present MST 390 kA improved confinement, and (*e*) present MST 210 kA improved confinement.

The total beta, $\beta_{\rm tot} \equiv 2\mu_0[\int (n_e T_e + n_i T_i)\, dV / \int dV]/B^2(a)$, is compared in Table I. The poloidal beta, β_θ, is similarly defined but with $B^2(a)$ replaced by $B_\theta^2(a)$. In standard plasmas, $B_\theta(a) \gg B_\phi(a)$, and $\beta_\theta \approx \beta_{\rm tot}$, but in plasmas with auxiliary poloidal current drive, $B_\phi(a)$ becomes significant, and $\beta_\theta > \beta_{\rm tot}$. With improved confinement, both $\beta_{\rm tot}$ and β_θ increase substantially. The improved-confinement betas at 210 kA are the largest yet achieved in the MST.

The τ_E of 10 ms at 210 kA significantly exceeds for the first time the scaling prediction of Connor and Taylor, where τ_E increases at constant beta and scales as $a^2 I_\phi^3 / N^{3/2}$, where $N = \pi a^2 \langle n_e \rangle$ is the line density. This scaling is derived assuming that resistive fluid turbulence (g-modes) limits RFP energy confinement [13]. In Fig. 4 are confinement data from different RFP devices. Most of these data were taken from Table I in [14], but the datum for TPE-1RM20 was taken from [15], and the data for the MST (*a*)–(*e*) are from the plasmas described in this Letter and from previously reported improved-confinement plasmas [5,6]. The diagonal line is the best fit to the data listed in [14], $\tau_E = 10.2(a^2 I_\phi^3 / N^{3/2})$. The previously achieved confinement times in the RFP have fallen on or somewhat below the prediction of Connor-Taylor. The assumption of confinement limited by resistive fluid turbulence has not been verified experimentally. The fact that improved-confinement MST plasmas now exceed the scaling indicates that either the scaling is not generally valid or possibly that the assumed limiting turbulence has been reduced. Another confinement scaling, $\tau_E = (1.9 \times 10^{-5}) a^{1.4} \mu^{0.29} Z_{\rm eff}^{-0.42} I_\phi^{0.34}$, where μ is the ion to proton mass ratio, is derived from nonlinear magnetohydrodynamic simulations of RFP plasmas without auxiliary current drive in which the core-resonant $m = 1$ magnetic fluctuations limit confinement [16]. Averaging over time and including sawtooth crashes, this scaling predicts $\tau_E < 1$ ms for MST parameters, which is significantly exceeded with the fluctuation reduction reported here.

In summary, we have demonstrated in the MST the need for simultaneous control of core and edge instability. With improved control of the surface parallel electric field, we have suppressed the edge-resonant $m = 0$ bursts observed in earlier auxiliary current drive experiments. This has allowed a further reduction of core-resonant $m = 1$ fluctuations and has resulted in a tenfold increase in the energy confinement time. With the goal of improving upon this result, we have begun tests of radio frequency current drive using both lower-hybrid and electron-Bernstein waves.

These plasmas deviate substantially from the Taylor relaxed state [1]. However, the edge current profile, e.g., is modified during improved confinement in a way roughly consistent with that observed in nonlinear MHD simulations where auxiliary current drive led to magnetic fluctuation reduction [17,18]. A more complete understanding of the $m = 1$ and $m = 0$ fluctuation reductions in these plasmas, as well as the relative contribution of each reduction to reduced energy transport, awaits ongoing upgrades to the MST profile diagnostics and plasma control techniques.

This work was supported by the U.S.D.O.E., including the Fusion Energy Postdoctoral Research Program administered by the Oak Ridge Institute for Science and Education.

*Electronic address: bchapman@facstaff.wisc.edu

[1] H. A. B. Bodin and A. A. Newton, Nucl. Fusion **20**, 1255 (1980).
[2] R. N. Dexter *et al.,* Fusion Technol. **19**, 131 (1991).
[3] J. S. Sarff *et al.,* Phys. Rev. Lett. **72**, 3670 (1994).
[4] J. S. Sarff *et al.,* Phys. Plasmas **2**, 2440 (1995).
[5] J. S. Sarff *et al.,* Phys. Rev. Lett. **78**, 62 (1997).
[6] M. R. Stoneking *et al.,* Phys. Plasmas **4**, 1632 (1997).
[7] B. E. Chapman, Ph.D. thesis, University of Wisconsin–Madison, Madison, 1997.
[8] G. Fiksel *et al.,* Phys. Rev. Lett. **72**, 1028 (1994).
[9] N. E. Lanier *et al.,* Phys. Rev. Lett. **85**, 2120 (2000).
[10] J. C. Reardon *et al.,* Rev. Sci. Instrum. **72**, 598 (2001).
[11] J. K. Anderson, Ph.D. thesis, University of Wisconsin–Madison, Madison, 2001.
[12] D. Craig *et al.,* Rev. Sci. Instrum. **72**, 1008 (2001).
[13] J. W. Connor and J. B. Taylor, Phys. Fluids **27**, 2676 (1984).
[14] K. A. Werley *et al.,* Nucl. Fusion **36**, 629 (1996).
[15] Y. Hirano *et al.,* Nucl. Fusion **36**, 721 (1996).
[16] J. Scheffel and D. D. Schnack, Phys. Rev. Lett. **85**, 322 (2000); Nucl. Fusion **40**, 1885 (2000).
[17] B. E. Chapman *et al.,* Phys. Plasmas **7**, 3491 (2000).
[18] C. R. Sovinec and S. C. Prager, Nucl. Fusion **39**, 777 (1999).